JTTEE5 22:744–755
DOI: 10.1007/s11666-013-9895-x
1059-9630/$19.00 © ASM International

Peer Reviewed

The Role of Spraying Parameters and Inert Gas Shrouding in Hybrid Water-Argon Plasma Spraying of Tungsten and Copper for Nuclear Fusion Applications

J. Matějíček, T. Kavka, G. Bertolissi, P. Ctibor, M. Vilémová, R. Mušálek, and B. Nevrlá

(Submitted October 23, 2012; in revised form January 11, 2013)

Tungsten-based coatings have potential application in the plasma-facing components in future nuclear fusion reactors. By the combination of refractory tungsten with highly thermal conducting copper, or steel as a construction material, functionally graded coatings can be easily obtained by plasma spraying, and may result in the development of a material with favorable properties. During plasma spraying of these materials in the open atmosphere, oxidation is an important issue, which could have adverse effects on their properties. Among the means to control it is the application of inert gas shrouding, which forms the subject of this study and represents a lower-cost alternative to vacuum or low-pressure plasma spraying, potentially applicable also for spraying of large surfaces or spacious components. It is a continuation of recent studies focused on the effects of various parameters of the hybrid water-argon torch on the in-flight behavior of copper and tungsten powders and the resultant coatings. In the current study, argon shrouding with various configurations of the shroud was applied. The effects of torch parameters, such as power and argon flow rate, and powder morphology were also investigated. Their influence on the particle in-flight behavior as well as the structure, composition and properties of the coatings were quantified. With the help of auxiliary calculations, the mass changes of the powder particles, associated with oxidation and evaporation, were assessed.

Keywords copper, gas shroud, hybrid plasma torch, influence of spray parameters, nuclear fusion, oxidation, tungsten

1. Introduction

Tungsten-based materials are among the candidates for plasma-facing components of fusion devices. Such components will be subject to high heat and particle fluxes from the hot plasma. Tungsten has a number of favorable characteristics for this application, namely refractory nature, high threshold for physical sputtering, good thermal conductivity, low vapor pressure, and does not react with hydrogen isotopes (Ref 1). Tungsten is proposed as the plasma-facing surface (armor), to be joined to underlying components—either copper-based heat sink or steel-based support structure. Plasma spraying is among the potential fabrication technologies, offering the following advantages:

– ability to coat large areas, including nonplanar shapes (compared with bulk or powder metallurgy technologies, limited in size and requiring an additional joining step), with sufficient thickness (of the order of mm, compared with atomic-level coating technologies, such as PVD and CVD, limited to microns);
– ability to repair damaged parts; and
– ability to form composites and graded layers to reduce stress concentration at the interface, with easy control of the compositional profile (Ref 1-3).

The main limitation is the relatively low thermal conductivity of plasma-sprayed layers, stemming from their layered structure, with imperfect bonding and voids between the layers (Ref 4).

In addition, W-Cu composites can find applications in heat dissipation components in microelectronic devices, or warhead materials in the military field (Ref 5).

During plasma spraying in air, oxidation of the metallic materials may take place to a various extent. The oxidation occurs principally in two stages (Ref 6):

– In flight, when the molten particles react with the mixture of plasma jet with surrounding atmosphere*; this

J. Matějíček, G. Bertolissi, P. Ctibor, M. Vilémová, R. Mušálek and **B. Nevrlá**, Department of Materials Engineering, Institute of Plasma Physics, Prague, Czech Republic; and **T. Kavka**, Department of Thermal Plasma, Institute of Plasma Physics, Prague, Czech Republic. Contact e-mail: jmatejic@ipp.cas.cz.

*It is worth noting that the water-stabilized plasma itself is a reducing environment, since there are two hydrogen species for each oxygen in H_2O molecules dissociated during plasma generation. However, plasma jets generated by this type of torch are characterized by strong entrainment of ambient air, which is the main factor in the in-flight oxidation.

stage is characterized by short duration (tens of ms) and high temperature (around the melting point).
– After the deposition, when the coating is exposed to air, at only moderately elevated temperatures, but longer duration (seconds to minutes).

The extent and relative contribution of these two stages, as well as the different oxidation mechanisms, depend on the spraying conditions and the sprayed materials.

During the in-flight stage, the oxidation process can advance by two principal mechanisms—diffusion and convection (Ref 6). According to Espie et al. (Ref 7), oxide/metal mixing due to strong convective movement is the dominant mechanism in gas-stabilized plasma spraying, while in the case of water-stabilized plasma, characterized by lower Reynolds number, surface oxidation dominates. Nevertheless, strong intermixing was observed in copper particles sprayed by hybrid water-argon-stabilized torch (WSP-H) (Ref 8), as well as arc-sprayed copper and plasma-sprayed steel (Ref 9). According to Syed et al. (Ref 10), the convective oxidation is more likely in the core of the plasma jet, while diffusion-controlled oxidation appeared to be the principal mechanism in the outer zone. The powder particle size has a strong effect, too. Smaller particles generally oxidize more than coarser ones, and also exhibit higher convective oxidation (Ref 11). Li et al. (Ref 12) found that for smaller particles, the in-flight oxidation was dominant, and the oxygen content in the coatings showed the same trend as in the free-flight particles; for larger particles, the post-impact oxidation was dominant and the oxygen content in the coating was relatively low and insensitive to particle size.

The in-flight oxidation of the particles modifies their melting properties (Ref 7). As the thermal diffusivity of the oxide is generally lower than that of the metal, its presence in the particle volume and/or surface slows down the heat exchange between the particle and the surrounding gases (Ref 13). In the specific case of tungsten, its oxides have lower boiling point than pure metal, and thus evaporate more easily. The oxide vapor cloud formed this way is thought to hinder thorough heating of the particles by the plasma jet (Ref 14). On the other hand, the same mechanism results in very low oxygen content in the coatings.

The oxidation phenomenon also affects the coating build-up and properties. When the particle composition is altered before their impact, the formation and layering of splats are different from those of pure metals (Ref 7). The oxidation effects on the coating properties can be both detrimental and advantageous. The coatings with higher oxide content can have higher porosity, lower ductility (Ref 9), or lower adhesive strength (Ref 15). In Ref 16, tungsten coating sprayed by APS and VPS are compared, showing about 3× lower oxide content, ~2× higher bond strength and thermal conductivity, ~1.1× higher hardness and ~1.5× better heat flux performance for the VPS coatings. In Ref 17, tungsten coatings sprayed in air and Ar atmosphere were compared, showing reduced porosity, improved intersplat bonding and thermal diffusivity for the latter. On the other hand, the oxides can result in higher hardness (Ref 9), improved wear resistance, superior compressive strength, or even better adhesion (Ref 10).

Together with the studies of oxidation mechanisms and effects, various methods of its suppression were investigated. These include adjustment of the spraying parameters (Ref 18-20), spraying in a closed chamber with controlled atmosphere or vacuum (Ref 21), shrouding of the plasma jet by inert (Ref 22) or reactive gas (Ref 6), and auto-shrouding by admixture of oxygen-consuming powder (Ref 19, 23).

The work presented in this article is a continuation of previous studies (Ref 8, 20) on the spraying of copper and tungsten by the WSP-H torch with combined water-argon stabilization (Ref 24). Their main results will be briefly summarized here. The first part was aimed at establishing the relationships between key torch/spraying parameters and the particle in-flight characteristics (first order process maps). The parameters under study included the torch power, flow of argon as the plasma-forming medium, and feeding and spraying distances. It was found that higher torch power led to both higher particle temperature and velocity, whereas higher argon flow rate increased the particle velocities with nearly no effect on their temperature. For copper, the particle plume was narrower for higher argon flow rates, larger extent of evaporation was observed for higher torch current. Particle temperatures and velocities had a direct influence on their in-flight oxidation. The oxide content in the free-flight particles decreased with the increasing argon flow rate, and correlated well with particle temperature and dwell time in the jet. Correspondingly, this affected the shapes and mutual bonding of the splats and consequently, the properties of the coatings. Increased torch power led to more contiguous, disk-shaped splats. Higher Ar flow reduced the splat splashing and generally resulted in larger splat diameters, due to higher impact velocity. The coatings built-up from such splats exhibited the lowest porosity and the highest thermal conductivity. The oxygen content in the coatings was slightly higher than in the free-flight particles, because of the post-deposition oxidation stage, but followed the same trend with respect to torch parameters. Inert gas shrouding was applied in a limited set of conditions. It reduced the in-flight oxidation of the particles significantly, while the effects on the coating oxygen content and properties were moderate. Tungsten exhibited principally the same trends of the in-flight particle properties with respect to torch settings as copper, but the coatings were found to be much less sensitive to the shrouding, possibly because of the already very low oxide content.

In the current study, the inert gas shrouding was applied over a wider torch operational space for both copper and tungsten. In addition, a smaller orifice was applied on the open end of the shrouding fixture, intended to limit the air entrainment in the fixture. Besides characterizing the in-flight oxidation, attention was paid to the mass losses of the particles, associated with evaporation and/or breakup, both experimentally and analytically. Finally, the properties of the coatings resulting from spraying with and without shrouding are compared.

2. Experimental

In this study, a hybrid plasma torch WSP-H (Institute of Plasma Physics, Prague, Czech Republic), using a (variable) mixture of water and argon as the plasma-forming media, was used. The arc current varied between 300 and 500 A,** and the argon flow rate was varied between 12 and 36 L/min. For these conditions, the torch total power was in the range of 60-135 kW. The spraying was carried out under both ambient and shrouded conditions. Inert gas shrouding was applied through a special shielding tube 280 mm in length and 250 mm in diameter, tightly attached to the front panel of the torch, enclosing the nozzle together with the anode (details in Ref 20). As air entrainment around the edges of the shield opening was observed, an additional front plate with a smaller orifice of 120-mm diameter was used in several cases. Argon was used as the shrouding gas in most cases. Three powders were used in the present experiments: water-atomized and air-atomized copper powders, both with granulometry between 100 and 125 μm (Stamont Metal International, Slovakia); and tungsten powder (Alldyne Powder Technologies, USA) with granulometry between 63 and 80 μm. Two types of copper powders were used because the powder used in the initial study became unavailable. On the other hand, this enabled the investigation of the powder morphology and oxygen content on their behavior during spraying. The powders were injected transversally into the plasma jet through a single injector under 70° angle to the torch axis at feeding distances 25 and 60 mm for tungsten and 60 and 90 mm for copper, using argon as a carrier gas. The powder feed rate was 17.1 kg/h for Cu and 27.1 kg/h for W powder, corresponding to the same volumetric values.

To study the in-flight oxidation, free-flight particles were collected from short spray runs into liquid nitrogen. Coatings were made on grit-blasted copper and carbon steel substrates (2.5 × 25 × 100 mm) on a water-cooled substrate holder. Deposition temperature, measured by a pyrometer between the spraying cycles, was kept around 100 °C by (a) preheating before deposition, and (b) adjustment of the water flow in the substrate holder, stationary argon jets pointing at the coated face and an additional air cooling between the torch passes. Typically, between 10 and 25 cycles were needed to form coatings with ~1-mm thickness.

Specific surface of the two copper feedstock powders was measured by the gas adsorption method (B.E.T.) at the Institute of Chemical Technology in Prague. As the specific surface of the air-atomized powder turned out to be below the resolution limit, it was estimated by calculation based on average particle diameter of 111 μm and spherical shape. Oxygen content of the feedstock powders, free-flight particles and copper coatings was determined by the inert gas fusion technique using a Leco TC 500 analyzer (Leco Corp., USA) at Unipetrol RPA. Morphological and structural observations of the free-flight particles and coatings were performed in an EVO MA15 scanning electron microscope—SEM (Carl Zeiss, Germany) in a backscattered and/or secondary electron modes. In selected points, elemental analysis was performed by energy-dispersive spectroscopy (EDS) in the SEM, using an XFlash 5010 detector (Bruker, Germany).

Particle size analysis was performed on the feedstock powders and free-flight particles, to assess quantitatively the material losses occurring during the spraying. Since the amount of powder needed for the analysis was much smaller than the initial collected amount, it was needed to choose the correct way of sampling to obtain a sample that would be representative of the whole collected batch. Three sampling methods were used: random sampling,

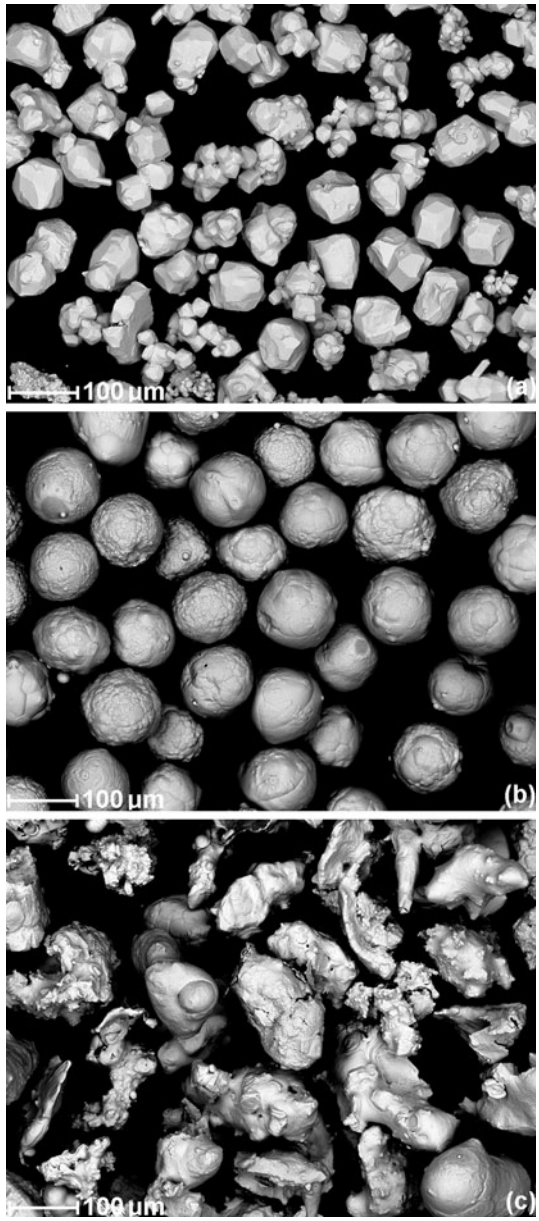

Fig. 1 Morphologies of the feedstock powders: (a) tungsten, (b) air-atomized copper, (c) water-atomized copper

**While 300 A was previously found optimal for spraying of copper and 500 A for tungsten, intermediate settings were also investigated for the sake of potential composite formation.

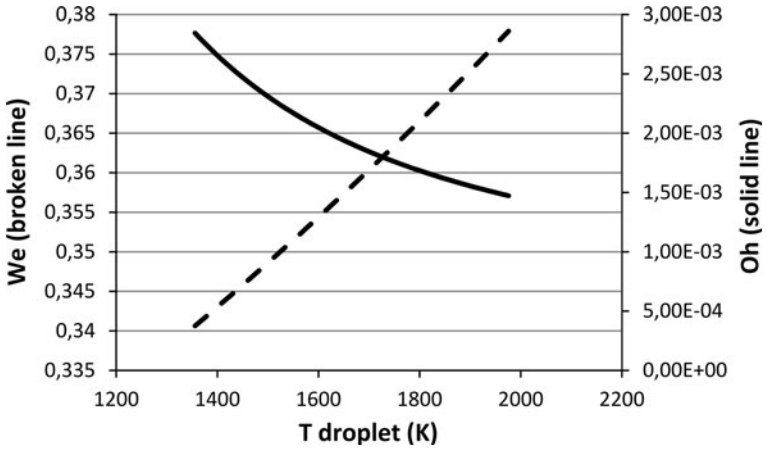

Fig. 2 Calculated values of *We* and *Oh* for a Cu droplet

quartering and moving sample division (adaptation of the rotating riffler sampling) (Ref 25). These three methods were applied on the air-atomized copper powder, and the differences between the results were statistically insignificant. Therefore, the random sampling method was used for collecting all the other samples. Four samples per batch were collected, and nine SEM images for each sample were taken, with a resolution of 1024 × 768 pixels and a scale of 1.976 μm per pixel. The images were analyzed using ImageJ software, with appropriate tools and plug-ins to determine the particles' geometrical features: the particle area, circularity and aspect ratio (Ref 26). From these, the equivalent diameter and equivalent volume were calculated according to eqns. 1-3, to allow size comparison for nonspherical particles:

equivalent diameter :

$$d_{\text{particle}} = \sqrt{\frac{4A}{\pi}} \quad \text{(Eq 1)}$$

aspect ratio:

$$\text{AR} = \frac{a_{\text{major}}}{a_{\text{minor}}} \quad \text{(Eq 2)}$$

equivalent volume:

$$V = \frac{4}{3}\pi\left(\frac{d_{\text{particle}}}{2}\right)^3 \quad \text{if AR<1.5}$$

$$V = \frac{4}{3}\pi\left(\frac{a_{\text{major}}}{2}\right)\left(\frac{a_{\text{minor}}}{2}\right)^2 \quad \text{if AR} \geq 1.5 \quad \text{(Eq 3)}$$

Porosity of the coatings was quantified by the Archimedean method. Thermal diffusivity and conductivity were determined by the xenon flash method on free standing coating samples between 100 and 400 °C, using an FL-3000 instrument (Anter Corp., USA). In-plane Young's modulus was determined by 4-point bending in an Instron 1362 universal testing machine with a 8800 control unit (Instron, UK) up to a small coating strain of 0.05%, to avoid stress-induced property changes (Ref 27).

Since the particle size analysis—aimed at assessment of the material loss due to evaporation—compared the volumes of the powders before and after spraying, it was important to consider the possibility of particle fragmentation during flight, in the liquid phase. The assessment of this phenomenon is described in the Appendix.

3. Results

3.1 In-flight Particle Evaporation, Fragmentation and Oxidation

Morphologies of the feedstock powders are shown in Fig. 1. The dominant shape of the tungsten powder is angular, nearly equiaxial; some particles appear as agglomerates of smaller particles. The air-atomized copper powder is mostly spherical. Particles of the water-atomized copper powder have irregular, ''blobby'' shape. Compared with the air-atomized powder, particles of the same ''diameter'' have lower volume. Specific surface of the air- and water-atomized powders is 0.006 and 0.055 m^2/g, respectively.

The results of modeling the Weber and Ohnesorge numbers for copper droplet are shown in Fig. 2. Since the critical values for deformation and fragmentation are $We \geq 0.6$ and $We \geq 12$, respectively, it can be concluded that under the conditions considered in the model, fragmentation in-flight does not occur. This is also supported by the measurements of in-flight particle characteristics in Ref 8, where no significant decrease of particle diameter over the measured distances was observed. However, possible fragmentation upon impact or breakup of the tungsten powder agglomerates cannot be completely ruled out.

Figure 3(a) shows the distributions of the copper feedstock powder (water-atomized) and the free-flight particles at several spraying conditions. The first thing to notice is a clear difference in shape between size distributions before and after spraying. While the starting

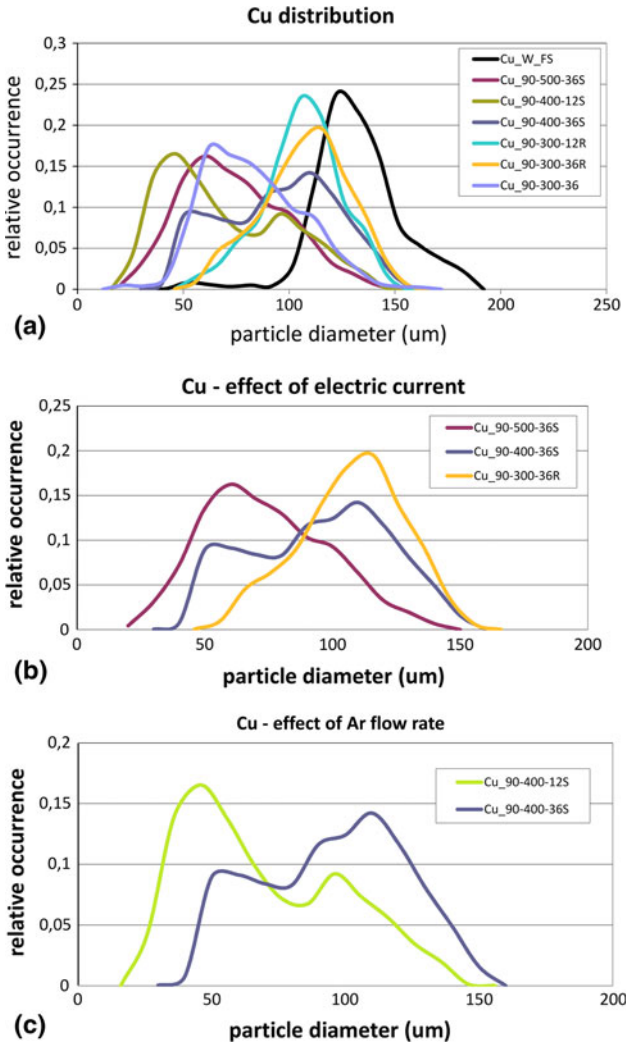

Fig. 3 (a) particle size distributions of the powders and free-flight particles sprayed at different conditions; these are labeled in the following order: feeding distance, torch current, flow rate of argon as a plasma forming gas; ''S'' denotes shrouding, ''R'' denotes shrouding with a reduced orifice; ''Cu-W FS'' denotes the water-atomized copper feedstock powder; (b) effect of the torch current on the copper free-flight particle sizes; (c) effect of the Ar flow rate on the copper free-flight particle sizes

Table 1 Equivalent diameters and volumes of copper feedstock powders and free-flight particles

Sample	Avg. equiv. diameter, μm	Avg. equiv. volume, μm^3
Cu-W FS	126.52	948,338
Cu 90-300-36	78.1	316,372
Cu 90-300-36R	102.67	635,052
Cu 90-400-36R	90.06	485,394
Cu 90-500-36S	68.99	239,269
Cu 90-400-12S	64.52	234,140
Cu 90-300-12R	100.93	591,353
Cu-A FS	108.60	678,360
Cu 90-300-36AR	101.48	607,819

Labels are the same as in Fig. 3, ''Cu-A'' denotes the air-atomized feedstock

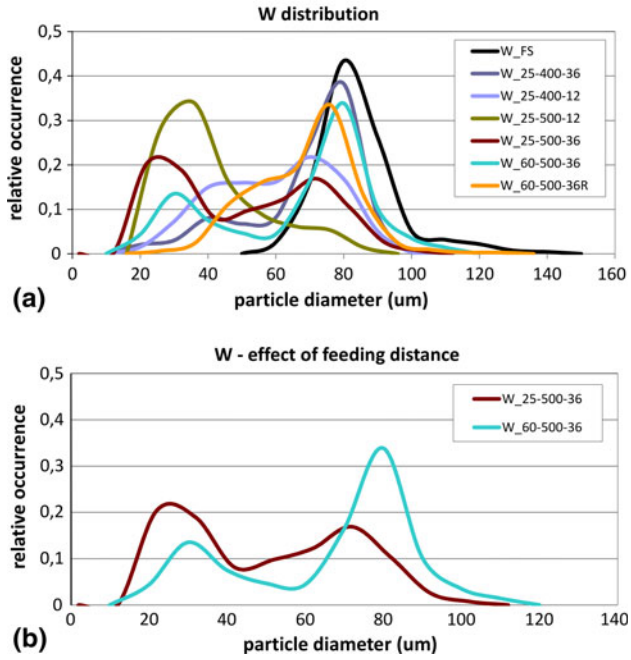

Fig. 4 (a) particle size distributions of the tungsten powder and free-flight particles sprayed at different conditions; (b) effect of the feeding distance on the tungsten free-flight particle sizes

Table 2 Equivalent diameters and volumes of tungsten feedstock powder and free-flight particles

Sample	Avg. equiv. diameter, μm	Avg. equiv. volume, μm^3
W FS	78.96	234,984
W 25-400-12	54.86	111,814
W 25-400-36	63.91	161,405
W 25-500-12	36.20	39,267
W 25-500-36	47.41	85,630
W 60-500-36	60.78	163,859
W 60-500-36R	63.23	154,848

Labels are the same as in Fig. 3

powder has a mono-dispersed distribution, the ones of sprayed particles became wider and, particularly for higher torch currents, apparently composed of two peaks. The one at higher values is close to the peak of the feedstock distribution, corresponding to particles that more or less conserve the initial mass, while the small difference is probably related to change in shape (spheroidization) upon melting. The peaks at lower values represent particles that effectively experience vaporization and mass loss in the plasma jet, the difference stemming likely from different trajectories in the jet.

The effects of different spraying conditions are summarized in Table 1. The nonspherical shape of the feedstock powders contributes to some uncertainty in determining the volume, and therefore, the comparison with sprayed particles should not be taken absolutely. However, the particles collected after spraying were

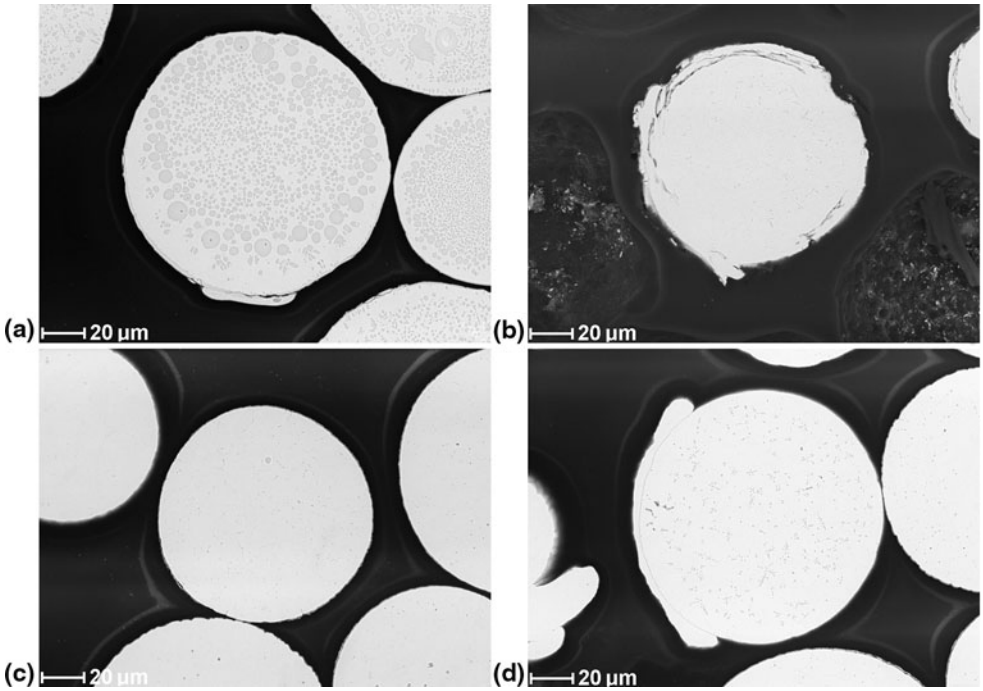

Fig. 5 Cross sections of the copper free-flight particles, sprayed at the 90-300-12 conditions: (a) open air, (b) shrouding, (c) shrouding + orifice, (d) shrouding + orifice, air-atomized powder

mostly spherical, so that their data could be more simply treated, and this permits at least a relative comparison of the different spraying conditions. Figure 3(b) illustrates the effect of electric current. Increased current leads to a decrease of the average particle size of particles, as well as change in the shape of the distributions. This happens because of higher specific enthalpy of the jet and higher heat input to the particles, which evaporate more quickly. When the Ar flow rate (Fig. 3c) is increased, particles experience a shorter dwell time inside the jet, and the amount of vaporized material is lower. When shrouding is applied, the reduction in particle size is relatively small. In this case, the phenomenon could be related to somewhat suppressed oxide formation, as the oxides might evaporate at a different rate than the base metal.

For the air-atomized powder, the feedstock size distribution was much narrower, and the average change due to spraying in the (shroud + orifice) conditions was very small—about 6%.

Figure 4(a) illustrates the size distributions for tungsten. Also in this case, splitting in two peaks is observed (to a different extent, depending on the spraying conditions). The average diameters are summarized in Table 2. The dependence on process parameters follows the same trends as for copper. Increasing the electric current results in an increased proportion of smaller particles; increasing the argon flow rate increased the amount of larger particles because the dwell time is decreased. For tungsten, the effect of the feeding distance was also evaluated (Fig. 4b). With increasing distance from the torch nozzle, the plasma temperature decreases quickly and particles experience less heating and vaporizing; therefore, smaller mass loss is observed.

In general, the evaporation phenomenon might be affected by the concurrent oxidation in flight as well, since the respective oxides have lower boiling point than the corresponding metals (Ref 20). However, attempt at quantitative assessment, e.g., comparison of the heat needed to vaporize a given amount of oxide versus metal, was hindered by the lack of available thermodynamic data for the former. The mass losses due to in-flight evaporation of course affect the deposition efficiency (DE). However, other factors also play a role at the point of impact; no clear correlation of the observed DE with the above characteristics was apparent.

Details of the copper free-flight particles collected in liquid nitrogen are shown in Fig. 5. Particles sprayed in air, Fig. 5(a) typically exhibit a well-discernible oxide phase, dispersed in a large number of inclusions, as an evidence of intense mixing in flight. The oxygen content in these particles, as determined by EDS, was around 9 wt.% ≅ 30 at.%, which corresponds to Cu_2O. In the base metal, it was around 0.5 wt.%; in the ''cap'' shown in Fig. 5(a) bottom, it was around 6 wt.%, indicating a finely intermixed zone. Majority of the particles sprayed in the shrouded conditions (Fig. 5b-d), did not contain any discernible oxide phase, except for fine, sub-micron granules in a few isolated particles. In a small minority of the particles, a sort of ''crust'' on the surface was observed (Fig. 5b). Its composition was the same as of the base metal, and hence, it did not originate from oxidation, but perhaps from the freezing action of the liquid nitrogen.

Table 3 Overview of the characteristics of the powders, free-flight particles (FFP) and coatings

Feeding distance, mm	Arc current, A	Argon flow, l/min	Shrouding	Powder	Oxygen—FFP, wt.%	Oxygen-coating, wt.%	Porosity, %	Thermal diffusivity, cm^2/s			E, GPa
								100 C	250 C	400 C	
				Cu-A-FS	0.70						
				Cu-W-FS	0.38						
				W-FS	0.02						
Copper											
60	300	36	no	Cu-W	1.50	2.24	8.4	0.147	0.132	0.125	58.05
90	300	12	no	Cu-W	2.07	3.04	4.7	0.115	0.097	0.085	101.3
90	300	24	no	Cu-W	1.11	1.74	13.0	0.107	0.103	0.097	49.7
90	300	36	no	Cu-W	0.57	1.06	13.3	0.148	0.137	0.138	
90	400	12	no	Cu-W	1.93	2.62	8.5	0.156	0.138	0.121	27.5
90	400	36	no	Cu-W	1.32	1.84	9.0	0.212	0.194	0.184	24.9
90	500	36	no	Cu-W	0.76	2.90	6.0	0.154	0.139	0.132	46.95
60	300	36	Ar	Cu-W	0.16	1.58	12.9	0.114	0.106	0.105	
90	300	12	Ar	Cu-W	0.24	1.93	9.9	0.097	0.093	0.096	48.9
90	300	24	Ar	Cu-W	0.25	1.14	15.1	0.152	0.146	0.153	31.55
90	300	24	Ar + 7%H2	Cu-W		1.18	14.8	0.108	0.100	0.099	
90	300	24	Ar 100	Cu-W		1.39	12.9	0.125	0.114	0.113	41.1
90	300	36	Ar	Cu-W	0.33	0.93	21.4	0.170	0.157	0.163	17.8
90	400	12	Ar	Cu-W	0.21						
90	400	36	Ar	Cu-W	0.16						
90	500	36	Ar	Cu-W	0.14	2.56	6.9	0.129	0.114	0.110	
60	300	36	Ar + R	Cu-W	0.21						
90	300	12	Ar + R	Cu-W	0.19	2.01	8.5	0.099	0.085	0.078	26.6
90	300	24	Ar + R	Cu-W	0.14	1.85	10.9	0.105	0.103	0.099	30.1
90	300	36	Ar + R	Cu-W	0.15	0.94	13.3	0.105	0.101	0.099	33.1
90	400	12	Ar + R	Cu-W	0.16						
90	400	36	Ar + R	Cu-W	0.16						
90	500	36	Ar + R	Cu-W	0.15						
90	400	36	Ar	Cu-A		1.54	8.5	0.157	0.148	0.140	35.0
90	300	12	Ar + R	Cu-A	0.27	1.94	8.9	0.110	0.100	0.094	25.1
90	300	24	Ar + R	Cu-A	0.24	1.76	11.0	0.114	0.106	0.101	29.9
90	300	36	Ar + R	Cu-A	0.33	1.17	9.9	0.142	0.148	0.139	26.5
90	400	36	Ar + R	Cu-A	0.20	1.85	6.4	0.180	0.169	0.162	39.8
90	500	36	Ar + R	Cu-A		1.91	7.3	0.342	0.329	0.332	31.5
Tungsten											
25	400	12	no	W	0.11		11.0	0.056	0.054	0.054	57.0
25	400	36	no	W	0.09		5.9	0.049	0.047	0.047	37.0
25	500	12	no	W	0.07		16.7	0.032	0.029	0.027	52
25	500	24	no	W	0.09		13.41	0.028	0.026	0.029	57.4
25	500	36	no	W	0.07		13.25	0.034	0.032	0.034	64.4
25	300	36	no	W			15.9	0.034	0.042	0.032	39.75
60	500	36	no	W	0.06						70.4
25	400	12	Ar	W			9.8	0.059	0.056	0.061	19.1
25	400	36	Ar	W			13.0	0.046	0.045	0.050	19.8
25	500	12	Ar	W							45.1
25	500	36	Ar	W			13.9	0.034	0.032	0.032	61.4
25	400	12	Ar + R	W	0.05						
25	400	36	Ar + R	W	0.05						
25	500	12	Ar + R	W	0.05		11.0	0.040	0.038	0.038	31.0
25	500	24	Ar + R	W	0.04		11.6	0.047	0.046	0.051	38.6
25	500	36	Ar + R	W	0.05		11.3	0.043	0.040	0.032	44.8
60	500	36	Ar + R	W	0.05						
Typical CV					2% W 4% Cu	1.5%	6%	0.5% W 0.8% Cu			15%

Ar denotes shrouding with argon at 210 L/min, except where noted; Ar + R shrouding with argon and the reduced orifice

Oxygen contents in the feedstock powders and in free-flight particles, together with other characteristics, are summarized in Table 3. The amount of oxygen in the air-atomized copper powder was about twice as much as in the water-atomized powder. Oxygen content in the tungsten powder was an order of magnitude lower, but still a measurable amount. Figure 6 illustrates the argon and shrouding effects for copper powders sprayed at 90-300 condition. When sprayed in air, the oxygen content changes from ~2 to ~0.5 wt.% when the Ar flow rate is increased from 12 to 36 L/min. In the shrouded conditions, the in-flight oxidation is significantly reduced, yielding about 0.3%. Further reduction (to about 0.15%) was achieved by the application of the smaller orifice,

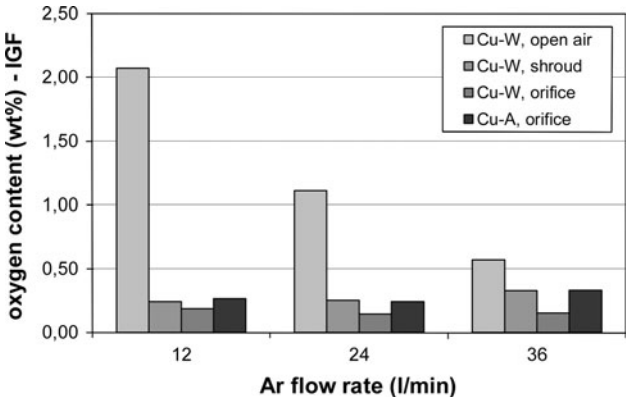

Fig. 6 Oxygen content in copper free-flight particles sprayed at 90-300 conditions (Cu-W = water-atomized, Cu-A = air atomized powder)

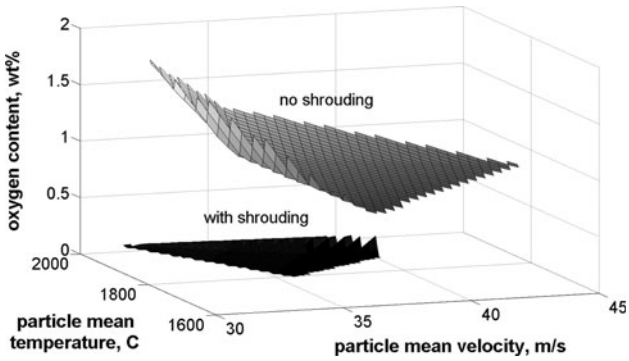

Fig. 7 Correlation of oxygen content in free-flight copper particles with their in-flight temperature and velocity (the latter data taken from Ref 8)

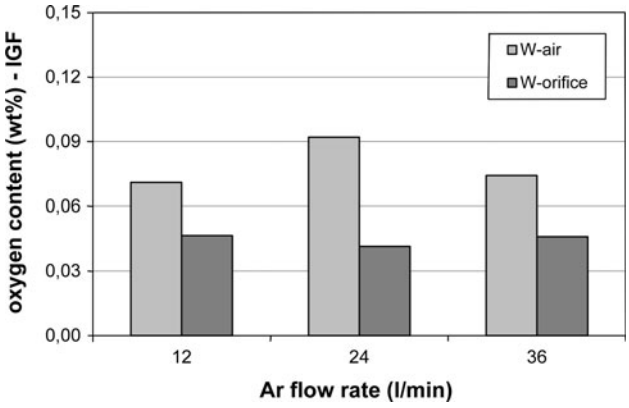

Fig. 8 Oxygen content in tungsten free-flight particles sprayed at 25-500 conditions

restricting the entrainment of air into the shroud. Since the air-atomized powder initially contained a higher amount of oxygen, its level after spraying for the more effective shrouding conditions (shroud + orifice) was about the same as for the water-atomized powder sprayed with the standard shroud only. In all the cases of shrouding,

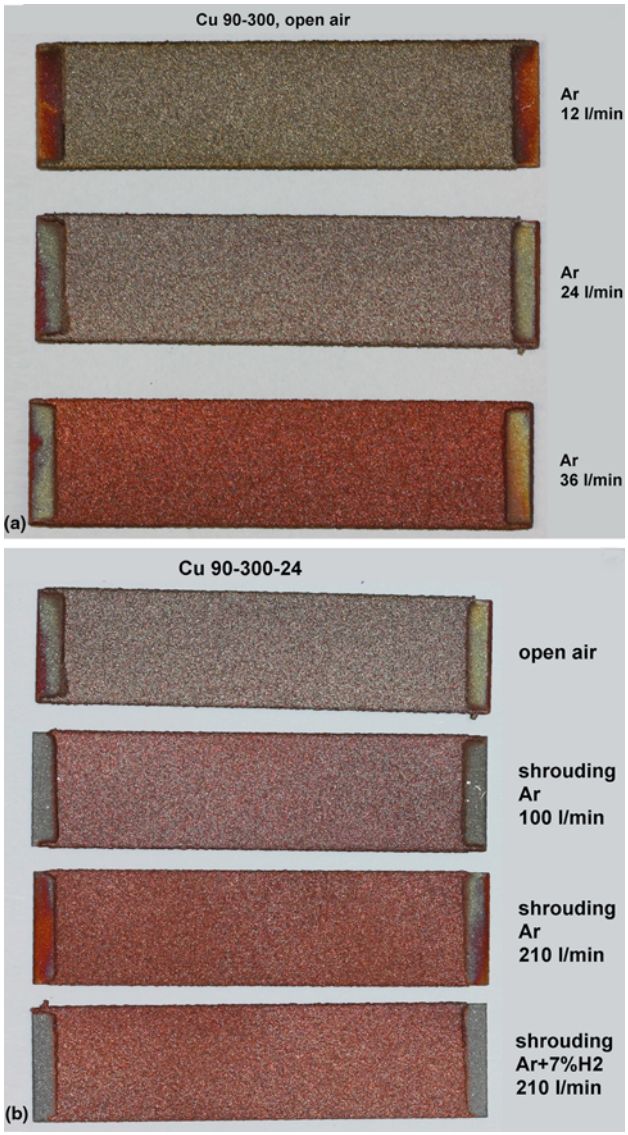

Fig. 9 Macroscopic appearance of the copper coatings, illustrating the color changes associated with different degrees of oxidation and the effects of (a) flow rate of argon as plasma-forming gas and (b) various shrouding modes. The brownish tint corresponds to the highest degree of oxidation and the reddish-orange to the lowest

there was no significant influence of the Ar flow rate and the unshrouded and shrouded trends tend to converge for higher Ar flow rates. For all the shrouded conditions, the oxygen content was lower than in the starting powders, testifying to the reducing effect of the plasma jet itself. In the unshrouded conditions, higher particle temperatures (achieved either by higher torch power or by shorter feeding distance) led to higher oxygen content (Table 3), whereas for the shrouded conditions, their effect was negligible.

Figure 7 illustrates the correlation of oxygen content in the free-flight copper particles with their temperature and velocity (a second-order process map). For the open-air

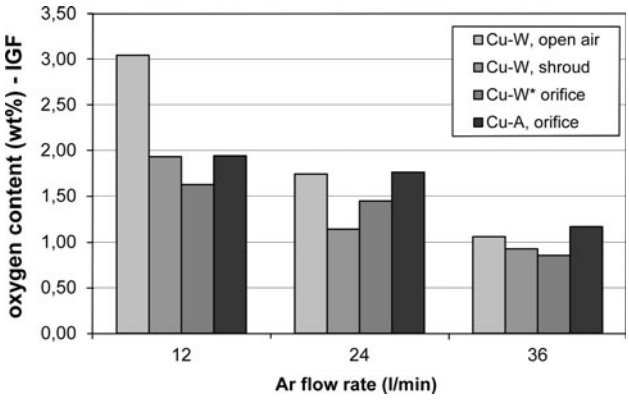

Fig. 10 Oxygen contents in selected Cu coatings (Cu-W = water-atomized, and Cu-A = air atomized powder). Since the data for the Cu-W shroud + orifice were not experimentally available, the values presented here (marked with an asterisk) were estimated from the Cu-W starting oxygen content and assuming the same increase due to spraying as for Cu-A

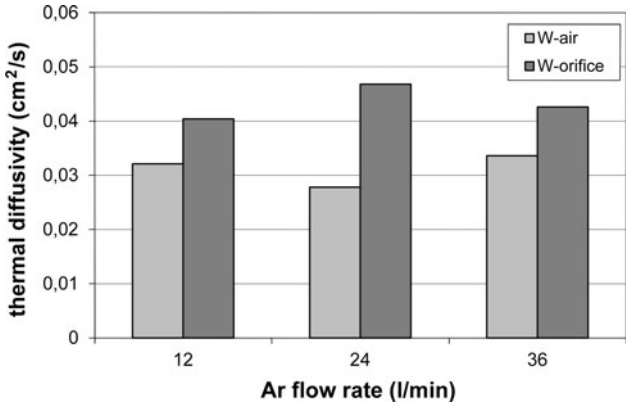

Fig. 11 Thermal diffusivity of selected W coatings

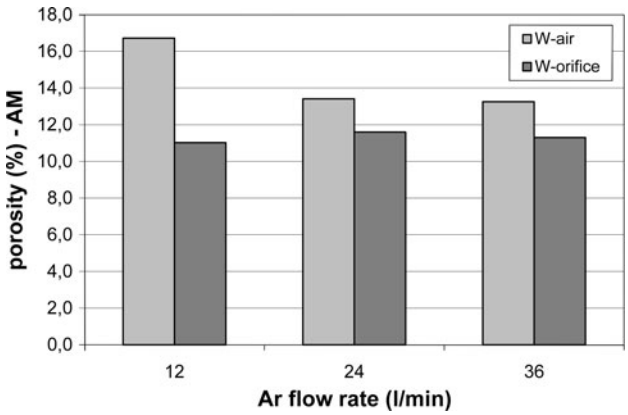

Fig. 12 Porosity in selected W coatings, determined by the Archimedean method

conditions, the expected trend is confirmed, i.e., the particles oxidize more the higher their temperature and longer dwell time in the jet (lower velocity). In the shrouded conditions, the influence of these variables was weaker, since the oxygen content was quite low in all cases.

For the tungsten powder, oxygen content in the free-flight particles (Fig. 8) was slightly higher than in the feedstock, but still very low. No clear trend is observed with respect to Ar flow rate, but an overall reduction with the application of shroud + orifice can be seen.

3.2 Coating Properties

Macroscopic appearance of the copper coatings with different degree of oxidation is shown in Fig. 9, illustrating the effects of Ar flow rate and shrouding. Oxygen contents in selected copper coatings are shown in Fig. 10. A positive effect of both the increased Ar flow rate and the shrouding, as already indicated in Ref 20, can be clearly seen. Quantitatively, the argon effect is stronger within the studied range than that of shrouding. There was little difference between effect of the plain shroud and the shroud with a reduced orifice. The higher oxygen content of the air-atomized powder translated into higher content in the coatings as well. It is worth noting that in the open-air conditions, the contributions of the in-flight and post-impact oxidation stages were similar. On the other hand, the application of shrouding suppressed the in-flight stage significantly, and, therefore, the contribution of the second stage was comparably higher.

As shown in Ref 8, the oxides were inhomogeneously distributed throughout the coatings, either as small globules intermixed with the metal inside the splats, or as thin layers on splat surfaces. Cu_2O was the dominant phase, and traces of CuO were also detected by x-ray diffraction. However, varying contrast in the SEM images suggested the presence of nonstoichiometric compositions, either as ''freezed-in'' solutions or ultrafine mixtures.

A relatively small variation in coating thermal diffusivity and Young's modulus was observed (see Table 3). Coating porosity, as determined by the Archimedean method, showed somewhat higher variation, but without clear trends. There was a general tendency toward higher diffusivity for higher Ar flow rate and for the shrouded conditions. However, the data scatter precludes stating this as a universal trend. The highest diffusivity was found in the coatings sprayed at the 90-500-36 (shrouding + orifice) conditions, which corresponded to the highest in-flight temperature and velocity (Ref 8). Thermal diffusivity values of copper coatings generally showed a slight decrease with measurement temperature, whereas tungsten coatings (below) exhibited a nearly constant dependence.

In tungsten coatings, no oxide was observed as a discernible phase. x-ray diffraction measurements on WSP-sprayed tungsten coatings (Ref 19) indicated similar values as those presented in Fig. 8. For this reason, and the inability to melt tungsten in the IGF method, oxygen determination in the current tungsten coatings was not attempted.

Figures 11 and 12 show the influence of Ar flow rate and shrouding on thermal diffusivity and porosity, respectively, of W coatings sprayed at 500 A and feeding distance of 25 mm. The application of shrouding generally

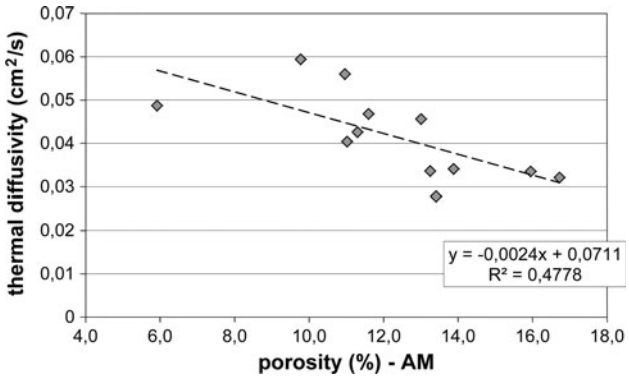

Fig. 13 Correlation between thermal diffusivity and open porosity of for evaluated W coatings

led to higher diffusivity and lower porosity, although the differences were smaller than those observed for copper. The Ar flow rate effect was even less pronounced, and the tendency was not preserved for all the studied conditions. Figure 13 indicates that these two characteristics are moderately correlated; however, there are generally more factors that influence the diffusivity than just porosity volume—namely, the distributions of pore sizes, shapes and orientations (Ref 4). A detailed analysis in Ref 17 indicated that the presence of oxides at the interfaces had much weaker effect on diffusivity than the imperfect intersplat contacts. Young's modulus, being an indirect indication of intersplat bonding quality, did not show very distinct trends with respect to spraying parameters, and the values were quite similar to those observed in WSP-sprayed coatings.

4. Conclusions

Copper and tungsten powders were sprayed by the hybrid water-argon torch, and the influences of several spraying parameters was investigated. These included the torch power, Ar flow rate, feeding distance, and the application of shrouding enclosure with or without a reduced orifice. All of these factors influence the in-flight particle temperatures and velocities, the course and extent of melting, evaporation and oxidation, and the properties of the resultant coatings. Owing to different thermal properties of these two materials, different values of the torch power and the feeding distance were found optimal for copper and tungsten, to achieve dense and conductive coatings desired for thermal management applications. When spraying composites, the individually optimized feeding parameters can be used for each powder, but single torch settings have to be used. Increased argon flow rate was generally found beneficial in all the above aspects. This is attributed to increased velocity and laminarity of the plasma jet, which shortens the dwell time of the particles and reduces the air entrainment in the jet. Tungsten was generally less sensitive to these parameters than copper. The application of inert gas shrouding, tightly attached to the torch front, was found to effectively reduce the extent of in-flight oxidation, even further when a reduced outlet orifice was used. In all such cases, the oxygen content in the free-flight particles was lower than that in the starting powders. This testifies that the plasma jet itself has a reducing effect and that the in-flight oxidation happens mainly because of its mixing with the surrounding atmosphere. For the two different copper powders, the initial oxygen content appeared more significant than the powder morphology. Despite the usage of inert gas jets aimed at the coated surface, the post-deposition oxidation stage was still relatively significant, lessening somewhat the positive effect of the jet shrouding. Size analysis of the free-flight particles indicated quite a significant mass loss due to in-flight evaporation, with consequences for the deposition efficiency as well as coating properties. This was strongly correlated with the spraying conditions, and might be influenced by the in-flight oxidation as well. The effects of the abovementioned factors on coating characteristics, such as oxygen content, porosity, thermal diffusivity and Young's modulus were quantified. The overall beneficial effects of increased Ar content in the plasma and of the inert gas shrouding were demonstrated, showing again higher sensitivity for copper than for tungsten.

Acknowledgments

Financial support received through grants no. FR-TI2/702 (Czech Ministry of Industry and Trade) and no. TA01010300 (the Technology Agency of the Czech Republic) is gratefully acknowledged.

Appendix: Assessment of Particle Fragmentation

According to studies on the behavior of droplets injected inside a cross-flow jet (Ref 28, 29), the key parameters which affect the deformation and fragmentation mechanisms are summarized in two nondimensional numbers: Weber (*We*), and Ohnesorge (*Oh*) numbers (Ref 28). Weber number is a measure of the relative importance of the fluid's inertia compared with its surface tension and in this case gives an idea of the interaction between fluid and liquid droplet; Ohnesorge number relates the viscous forces to inertial and surface tension forces and represents the simplicity to break the droplet into smaller ones. The definitions are shown below:

$$We = \frac{\rho_g v_{rel}^2 D_0}{\sigma_d} \quad \text{(Eq 4)}$$

$$Oh = \frac{\mu_d}{\sqrt{\rho_d v_{rel} \sigma_d}} \quad \text{(Eq 5)}$$

where ρ_g = plasma density, v_{rel} = relative velocity, D_0 = droplet initial diameter, σ_d = droplet surface tension, ρ_d = droplet density, μ_d = droplet dynamic viscosity

Table 4 Input data for Weber and Ohnesorge numbers for copper (Ref 8, 32)

Input Data	@500 A, 36 L/min Ar, 120 mm from torch exit
Plasma density, kg/m^3	0.707718
Plasma velocity, m/s	89
Droplet Velocity, m/s	35
Droplet diameter, m	$200*10^{-6}$
Droplet viscosity, mPa s (Copper UNS C10100)	$\eta = \eta_0 \cdot 10^{\left(-a_2+\frac{a_2}{T}\right)}$ $a_1 = 0.4420$ $a_2 = 1393.4$ $\eta_0 = 1\,\text{mPa s}$
Droplet density, kg/m^3 (Copper UNS C10100)	$\rho = c_1 - c_2(T - T_{\text{ref}})$ $c_1 = 7997\frac{\text{kg}}{\text{m}^3}$ $c_2 = 0.819\frac{\text{kg}}{\text{m}^3\text{K}}$ $T_{\text{ref}} = 1357.7\,\text{K}$
Droplet surface tension, mN m (Ref 31)	$\sigma = 1257 - 0.20(T - 1356)$

Once the variables affecting the phenomenon are defined, critical values for deformation and fragmentation should be identified. According to Ref 29, it appears that for low viscosities of the liquid phase (that means values of $Oh < 0.1$) the liquid droplet does not behave as a sphere when $We > 0.6$. Furthermore, fragmentation happens when $We \geq 12$. Different break-up mechanisms and corresponding We values were presented in Ref 30. If the liquid phase has higher viscosity, resulting in a higher value of the Ohnesorge number $Oh > 0.1$, the conditions to reach deformation and fragmentation of a droplet are more difficult and the Weber number should then be much higher to reach them.

In order to calculate the parameters presented above, thermodynamic values relevant for the current plasma spraying conditions are needed:

torch-related parameters: arc current and Ar flow rate, which affect the plasma jet velocity, temperature, density and other physical properties;

parameters of the spraying setup: feeding distance, distance (from torch exit) in which approximately copper particles melt;

feedstock-related parameters: copper particles velocity and size distribution (at injection and melting distances).

Since all these data were not available exactly, for evident experimental limits, some approximation had to be made, with the best estimation of values and using the safety overestimating principle. The following parameters were considered:

Among all conditions used in the spraying, only the one with arc current $I = 500$ A was considered because it is the one which gives the highest amount of energy to the plasma jet, so if deformation and fragmentation do not happen in this case, they will not happen with lower energies. The Ar gas flow rate taken for calculations was 36 L/min (the highest value of the experimental conditions), because increasing the amount of argon increases the momentum transferred to the particles/droplets, so if droplets do not fragment in these conditions, they will not fragment at weaker conditions. The axial distance used to obtain the values of temperature and velocities of plasma and droplets was set at 120 mm from the torch exit, since the injection was made at 60-90 mm and at 120 mm, the particles were reasonably melted, conserving a relatively high temperature and velocity (if data were not available for this distance, interpolations were made from the available data). The particle size was again slightly overestimated; since at 200 μm, fragmentation would be more likely than at 125 μm. Temperature range of the copper droplet between 1356 and 2576 K was considered. The input data used in the calculations are summarized in Table 4.

References

1. J. Matějíček, P. Chráska, and J. Linke, Thermal Spray Coatings for Fusion Applications—Review, *J. Therm. Spray Technol.*, 2007, **16**(1), p 64-83
2. J. Matějíček, Y. Koza, and V. Weinzettl, Plasma Sprayed Tungsten-Based Coatings and Their Performance Under Fusion Relevant Conditions, *Fus. Eng. Des.*, 2005, **75-9**, p 395-399
3. J. Matějíček, and R. Mušálek, Processing and properties of plasma sprayed W + Cu composites, *Thermal Spray Crossing Borders (Proc. Intl. Thermal Spray Conf.)*, E. Lugscheider, Ed., DVS Verlag, Maastricht, 2008, p 1412-1417
4. M. Vilémová, J. Matějíček, R. Mušálek, and J. Nohava, Application of Structure-Based Models of Mechanical and Thermal Properties on Plasma Sprayed Coatings, *J. Therm. Spray Technol.*, 2012, **21**(3-4), p 372-382
5. H.K. Kang and S.B. Kang, Behavior of Porosity and Copper Oxidation in W/Cu Composite Produced by Plasma Spray, *J. Therm. Spray Technol.*, 2004, **13**(2), p 223-228
6. D. Kolman and K. Voleník, Modeling of Oxidation During Plasma Spraying of Iron Particles, *Plasma Chem. Plasma Process.*, 2002, **22**(3), p 437-450
7. G. Espie, A. Denoirjean, P. Fauchais, J.C. Labbe, J. Dubsky, O. Schneeweiss, and K. Volenik, In-Flight Oxidation of Iron Particles Sprayed Using Gas and Water Stabilized Plasma Torch, *Surf. Coat. Technol.*, 2005, **195**(1), p 17-28
8. T. Kavka, J. Matějíček, P. Ctibor, A. Mašláni, and M. Hrabovský, Plasma Spraying of Copper by Hybrid Water-Gas Dc Arc Plasma Torch, *J. Therm. Spray Technol.*, 2011, **20**(4), p 760-774
9. K. Murakami, N. Fujita, S. Adachi, H. Nakajima, and H. Miyake, Oxidation of Thermal Sprayed Metallic Materials During Flying in Air and the Coating Structures, *Mater. Sci. Forum*, 2004, **449-4**, p 1301-1304
10. A.A. Syed, A. Denoirjean, P. Denoirjean, J.C. Labbe, and P. Fauchais, In-Flight Oxidation of Stainless Steel Particles in Plasma Spraying, *J. Therm. Spray Technol.*, 2005, **14**(1), p 117-124
11. A.A. Syed, A. Denoirjean, P. Fauchais, and J.C. Labbe, On the Oxidation of Stainless Steel Particles in the Plasma Jet, *Surf. Coat. Technol.*, 2006, **200**(14-15), p 4368-4382
12. C.J. Li and W.Y. Li, Effect of Sprayed Powder Particle Size on the Oxidation Behavior of MCrAlY Materials During High Velocity Oxygen-Fuel Deposition, *Surf. Coat. Technol.*, 2003, **162**(1), p 31-41
13. V.V. Sobolev and J.M. Guilemany, Oxidation of Coatings in Thermal Spraying, *Mater. Lett.*, 1998, **37**(4-5), p 231-235
14. J. Matějíček, K. Neufuss, D. Kolman, O. Chumak, and V. Brožek, Development and Properties of Tungsten-Based Coatings Sprayed by WSP(R), *Thermal Spray Connects: Explore Its Surfacing Potential! (Proc. International Thermal Spray Conference)*, E. Lugscheider, Ed., DVS, Basel, 2005, p 634-640
15. W.Y. Li, C.J. Li, and H.L. Liao, Significant Influence of Particle Surface Oxidation on Deposition Efficiency, Interface Microstructure and Adhesive Strength of Cold-Sprayed Copper Coatings, *Appl. Surf. Sci.*, 2010, **256**(16), p 4953-4958

16. D.Y. Hu, X.B. Zheng, Y.R. Niu, H. Ji, F.L. Chong, and J.L. Chen, Effect of Oxidation Behavior on the Mechanical and Thermal Properties of Plasma Sprayed Tungsten Coatings, *J. Therm. Spray Technol.*, 2008, **17**(3), p 377-384
17. S. Boire-Lavigne, C. Moreau, and R.G. Saint-Jacques, The Relationship Between the Microstructure and Thermal-Diffusivity of Plasma-Sprayed Tungsten Coatings, *J. Therm. Spray Technol.*, 1995, **4**(3), p 261-267
18. W.J. Lenling, J.A. Henfling, and M.F. Smith, Method for Minimizing Decarburization and Other High Temperature Oxygen Reactions in a Plasma Sprayed Material, Patent US5217746, 1993
19. J. Matějíček, V. Weinzettl, E. Dufková, V. Piffl, and V. Peřina, Plasma Sprayed Tungsten-based Coatings and their Usage in Edge Plasma Region of Tokamaks, *Acta Technica CSAV*, 2006, **51**(2), p 179-191
20. T. Kavka, J. Matějíček, P. Ctibor, and M. Hrabovský, Spraying of Metallic Powders by Hybrid Gas/Water Torch and the Effects of Inert Gas Shrouding, *J. Therm. Spray Technol.*, 2012, **21**(3-4), p 695-705
21. G. Mauer, R. Vassen, and D. Stover, Controlling the Oxygen Contents in Vacuum Plasma Sprayed Metal Alloy Coatings, *Surf. Coat. Technol.*, 2007, **201**(8), p 4796-4799
22. M. Jankovic, J. Mostaghimi, and V. Pershin, Design of a New Nozzle for Direct Current Plasma Guns with Improved Spraying Parameters, *J. Therm. Spray Technol.*, 2000, **9**(1), p 114-120
23. K. Neufuss, V. Brožek, and J. Matějíček, Tungsten-based Protective Coating and Method of its Preparation (in Czech), Patent CZ303411, 2012
24. T. Kavka, J. Gregor, O. Chumak, and M. Hrabovský, Effect of Arc Power and Gas Flow Rate on Properties of Plasma Jet Under Reduced Pressures, *Czech J. Phys.*, 2004, **54**, p C753-C758
25. A. Jillavenkatesa, L. H. Lum, and S. Dapkunas, NIST Recommended Practice Guide: Particle Size Characterization, NIST SP-960-1, 2001
26. ImageJ, National Institute of Health, http://rsb.info.nih.gov/ij/
27. R. Mušálek, J. Matějíček, M. Vilémová, and O. Kovářík, Non-Linear Mechanical Behavior of Plasma Sprayed Alumina Under Mechanical and Thermal Loading, *J. Therm. Spray Technol.*, 2010, **19**(1-2), p 422-428
28. F.O. Bartz, D.R. Guildenbecher, R. Schmehl, R. Koch, H.-J. Bauer, and P.E. Sojka, Model Comparison for Single Droplet Fragmentation Under Varying Accelerations, *24th European Conference on Liquid Atomization and Spray Systems*, Estoril, Portugal, 2011
29. L.-P. Hsiang, and G.M. Faeth, Drop Deformation and Breakup Due to Shock Wave and Steady Disturbances, *32th Aerospace Sciences Meeting and Exhibit,* American institute for Aeronautics and Astronautics, Reno, NV, 1994, paper no. 94-0560
30. T. Aoyama, Y. Hattori, J. Mizuta, and Y. Sato, An Experimental Study on Premixed-Charge Compression Ignition Gasoline Engine, SAE Technical Paper 960081, 1996
31. T. Matsumoto, H. Fujii, T. Ueda, M. Kamai, and K. Nogi, Measurement of Surface Tension of Molten Copper Using the Free-Fall Oscillating Drop Method, *Meas. Sci. Technol.*, 2005, **16**(2), p 432-437
32. M. Hrabovský, V. Kopecký, V. Sember, T. Kavka, O. Chumak, and M. Konrád, Properties of Hybrid Water/Gas DC Arc Plasma Torch, *IEEE Trans. Plasma Sci.*, 2006, **34**(4), p 1566-1575